JVI Journals.ASM.org

Merkel Cell Polyomavirus Small T Antigen Targets the NEMO Adaptor Protein To Disrupt Inflammatory Signaling

David A. Griffiths,[a,b] Hussein Abdul-Sada,[a,b] Laura M. Knight,[a,b] Brian R. Jackson,[a,b] Kathryn Richards,[a,b] Emma L. Prescott,[a,b] A. Howard S. Peach,[c] G. Eric Blair,[a] Andrew Macdonald,[a,b] Adrian Whitehouse[a,b]

School of Molecular and Cellular Biology, Faculty of Biological Sciences,[a] and Astbury Centre for Structural Molecular Biology,[b] University of Leeds, Leeds, United Kingdom; Department of Plastic Surgery, Leeds Teaching Hospitals NHS Trust, St. James's University Hospital, Leeds, United Kingdom[c]

Merkel cell carcinoma (MCC) is a highly aggressive nonmelanoma skin cancer arising from epidermal mechanoreceptor Merkel cells. In 2008, a novel human polyomavirus, Merkel cell polyomavirus (MCPyV), was identified and is strongly implicated in MCC pathogenesis. Currently, little is known regarding the virus-host cell interactions which support virus replication and virus-induced mechanisms in cellular transformation and metastasis. Here we identify a new function of MCPyV small T antigen (ST) as an inhibitor of NF-κB-mediated transcription. This effect is due to an interaction between MCPyV ST and the NF-κB essential modulator (NEMO) adaptor protein. MCPyV ST expression inhibits IκB kinase α (IKKα)/IKKβ-mediated IκB phosphorylation, which limits translocation of the NF-κB heterodimer to the nucleus. Regulation of this process involves a previously undescribed interaction between MCPyV ST and the cellular phosphatase subunits, protein phosphatase 4C (PP4C) and/or protein phosphatase 2A (PP2A) Aβ, but not PP2A Aα. Together, these results highlight a novel function of MCPyV ST to subvert the innate immune response, allowing establishment of early or persistent infection within the host cell.

Merkel cell carcinoma (MCC) is an aggressive neuroendocrine carcinoma of the skin (1). Similar to other skin cancers, prolonged UV exposure is a known MCC risk factor, and incidence also increases sharply in the elderly (2). MCC is also dramatically increased upon the loss of immunocompetence and is more frequent in AIDS patients and organ transplant recipients (3, 4). As such, this etiology is reminiscent of other virus-induced cancers.

In 2008, Merkel cell polyomavirus (MCPyV) was identified as clonally integrated in ~80% of MCCs (5). It is the most recently discovered virus known to cause human cancer and the first human polyomavirus strongly linked with tumor induction (6, 7). Like other polyomaviruses, the MCPyV genome comprises early and late gene regions separated by a noncoding regulatory region. The early region encodes large T antigen (LT), small T antigen (ST), and 57kT proteins produced by alternative splicing (5).

A monoclonal viral integration pattern is observed in MCC, indicating that MCPyV infection and integration occur prior to clonal expansion of tumor cells (5). Additionally, truncating mutations in the integrated MCPyV LT render the virus replication defective, thus dismissing any passenger role of the virus in MCC tumorigenesis (6). Furthermore, ST and N-terminal regions of LT remain unaffected by tumor-derived mutations, suggesting that they also contribute to MCC tumorigenesis. This is supported by experiments showing that depletion of the T antigens leads to cell cycle arrest and cell death in MCPyV-positive MCC cell lines (8). This highlights that MCPyV ST and LT are important factors in regulating virus replication and play critical roles in human cell transformation. However, the molecular mechanisms implicating the MCPyV T antigens in virus replication and cancer development are yet to be fully elucidated.

Previous studies with related polyomaviruses, such as simian virus 40 (SV40), show that ST is required for upregulation of early viral promoter activity and also stimulates LT-mediated activation of the late viral promoter (9, 10). Furthermore, although SV40 ST expression alone is not capable of transforming cells, coexpression of SV40 ST and LT, together with the telomerase catalytic subunit hTERT and the oncogenic version of H-RAS, are sufficient to generate fully transformed human cells capable of tumor formation *in vivo* (11). SV40 ST activity is due to an interaction with protein phosphatase 2A (PP2A), the major cellular serine/threonine phosphatase. It associates with PP2A A and C subunits, displacing the regulatory B subunit, resulting in changes to PP2A substrate specificity and subsequent control of signaling pathways (12, 13).

In contrast, recent evidence suggests that MCPyV ST is oncogenic (14). Expression of ST alone is sufficient to transform rodent cells to anchorage- and contact-independent growth and also induces serum-free proliferation of human cells. Moreover, specific depletion of MCPyV ST is sufficient to inhibit MCPyV-positive MCC cell growth. Surprisingly, however, these effects were independent of the conserved interaction with PP2A (14). Uniquely, MCPyV ST deregulates cap-dependent translation by maintaining the hyperphosphorylated state of the eukaryotic translational regulatory protein, 4E-binding protein 1 (14). In addition, it targets the cellular ubiquitin ligase SCF^{Fwb7}, which stabilizes MCPyV LT and several cellular oncoproteins, such as c-Myc and cyclin E (15).

NF-κB is a pivotal family of transcription factors that regulate expression of numerous target genes with diverse roles ranging from inflammation and immunity to cell death or proliferation (16). The family consists of five structurally homologous members, forming a variety of homo- and heterodimers, including the

Received 5 August 2013 Accepted 4 October 2013
Published ahead of print 9 October 2013
Address correspondence to Adrian Whitehouse, a.whitehouse@leeds.ac.uk, or Andrew Macdonald, a.macdonald@leeds.ac.uk.

doi:10.1128/JVI.02159-13

most common heterodimer of RelA. NF-κB is found in an inhibited cytoplasmic form, maintained in this conformation by virtue of an interaction with members of the inhibitor of κB (IκB) family of proteins (17). NF-κB is activated in response to inflammatory stimuli by cytokines, such as tumor necrosis factor alpha (TNF-α) or by pattern recognition receptors (PRRs) that detect pathogen-associated molecular patterns (PAMPS). Engagement of the TNF-α receptor (TNFR) or PRRs initiates a coordinated signaling cascade, resulting in the activation of the IκB kinase (IKK) complex (18–20). This complex contains two catalytic kinase components, IKKα and IKKβ, as well as a noncatalytic regulatory subunit, NF-κB essential modulator (NEMO) or IKKγ. NEMO acts as a scaffold for the IKK complex and serves to recruit it to upstream signaling complexes. The activated IKK complex phosphorylates IκB, resulting in its rapid degradation, allowing the released NF-κB heterodimer to translocate to the nucleus and activate transcription of proinflammatory cytokines and upregulate expression of type I interferons (21).

Given the essential role for NF-κB activation in both the inflammatory and antiviral responses, it has emerged as a prime target for viral subversion. Virus proteins antagonize all stages of the NF-κB signaling pathway (22). Both the hepatitis C virus core and human papillomavirus E7 proteins inhibit IKK activation, preventing IκB degradation (23, 24). Human cytomegalovirus (CMV) and molluscum contagiosum poxvirus target NEMO to disrupt IKK activation. While the poxvirus MC159 protein inhibits IKK activation through an interaction with NEMO, conversely the CMV M45 protein redistributes NEMO to autophagocytic bodies, where it is degraded (25, 26). The African swine fever virus prevents NF-κB activation downstream of the IKK complex by encoding an IκB orthologue, replacing the host inhibitor upon IKK-induced degradation (27, 28). Alternatively, the myxovirus-encoded nuclear factor colocalizes with NF-κB in the nucleus to prevent induction of NF-κB-dependent genes (29). Interestingly, SV40 ST has been shown to upregulate NF-κB activation in a PP2A-dependent manner, although some proinflammatory targets, such as IL-8, are downregulated in the presence of SV40 ST (30). Intriguingly, however, the PP2A-independent transforming ability of MCPyV ST (14) suggests that alternative mechanisms of modulating NF-κB by MCPyV may be important.

In this study, we show that MCPyV ST negatively regulates NF-κB-mediated transcriptional activation. This effect is mediated through a novel interaction between MCPyV ST and NEMO. Specifically, MCPyV ST inhibits IKKα/IKKβ-induced IκB phosphorylation, limiting translocation of NF-κB into the nucleus. Regulation of this process involves a previously undescribed interaction between MCPyV ST and the cellular phosphatase subunits, PP4C and/or PP2A Aβ. These findings have important implications for virus replication and MCPyV-induced tumorigenesis, as MCPyV ST may interfere with the host innate immune response to enhance viral replication and persistence in the host cell.

MATERIALS AND METHODS

Plasmids, antibodies, and cells. The MCPyV ST was PCR amplified from MCC tumor genomic DNA using primers 5′-GGG GGT ACC ATG GAT TTA GTC and 5′-GGG CCC GGG CTA GAA A and cloned into the multiple cloning site of pEGFP-cI to generate pEGFP-ST. FLAG-tagged MCPyV small T antigens were also amplified and cloned into pCDNA5/frt/To to create iST-FLAG. The green fluorescent protein (GFP)-ST carboxy-terminal truncation series was PCR amplified from pEGFP-ST and cloned into the multiple cloning site of pEGFP-cI. pEGFP-ST R7A was PCR amplified from pEGFP-ST, incorporating the desired mutation in the forward primer. pGFP-STΔ95-111 and pGFP-STΔ111-128 deletion mutants were produced using the QuikChange site-directed mutagenesis kit (Stratagene), as directed by the manufacturer's instructions. Primer sequences for these deletion and site-directed mutations are available upon request. The MCPyV early promoter region was PCR amplified from MCC genomic DNA using the following primers: 5′-CAT CCT GAA AAA TAA ATA AGG ATA CTT ACT C and 5′-ATA ACA ATT AGG AGC AAT CTC CA. Primers incorporated KpnI and SmaI restriction sites, allowing the promoter to be inserted 5′ of the luciferase gene in pGL3-Basic, to generate pGL3-Early. Expression vectors for EE-PP2A Aβ and FLAG-PP4C were kindly provided by Stefan Strack, University of Iowa, and Marilyn Goudrealt, University of Toronto, respectively. Antibodies against NEMO (Abcam), LC3 (Cell Signaling), lamin B (Calbiochem), GAPDH (glyceraldehyde-3-phosphate dehydrogenase; Abcam), phospho-IκB (Cell Signaling), phospho-IKKα/IKKβ (Cell Signaling), p50 (Santa Cruz), p65 (Santa Cruz), FLAG (Sigma-Aldrich), Glu-Glu (Abcam), GFP (Living Colors), glutathione *S*-transferase (GST; Sigma-Aldrich), and β-actin (Sigma-Aldrich) were purchased from their respective suppliers. Western blotting and immunofluorescence analysis were carried out using specific antibodies at 1:1,000 and 1:250 dilutions, respectively.

HEK293, Huh7, and Flp-In 293 cells were maintained in Dulbecco's modified Eagle's medium (DMEM) containing 10% fetal bovine serum (FBS) and 1% penicillin-streptomycin. MCC13 and MKL-1 cell lines were maintained in RPMI 1640 media supplemented with 10% FBS and 1% penicillin-streptomycin. To generate the i293-ST inducible cell line, Flp-In 293 cells were cotransfected with iST-FLAG and pPGK/Flip/ObpA using Lipofectamine 2000 (Invitrogen) and selected by hygromycin B resistance at 100 μg/ml. ST-FLAG expression was induced with 2 μg/ml doxycycline hyclate for up to 48 h.

Immunoblotting. Cells were lysed in RIPA buffer (50 mM Tris-HCl at pH 7.6, 150 mM NaCl, 1% NP-40) and supplemented with a protease inhibitor cocktail (Roche). Proteins were separated by SDS-PAGE before transfer onto nitrocellulose membrane (Hybond C Extra; Amersham Biosciences). Membranes were probed with the appropriate primary and horseradish peroxidase (HRP)-conjugated secondary antibodies. Proteins were detected using EZ-ECL enhancer solution (Geneflow).

Quantitative real-time PCR arrays. Total RNA was harvested from uninduced or induced i293-ST cells by TRIzol extraction, before incubation with chloroform and precipitation by addition of isopropanol. RNA was treated for genomic DNA contamination using a DNase-free kit (Ambion), before purification using an RNeasy minikit (Qiagen). The SA Biosciences RT^2 first-strand kit (C-03; SA Biosciences) was used to produce cDNA. SA Biosciences RT^2 profiler PCR array system kits were used to perform the arrays, with plates containing signal transduction and cancer pathway finder primer sets. Quantitative real-time PCR was performed using a 7900 HT (ABI), with the manufacturer's software used to analyze results as previously described (31).

Determination of secreted IL-8 and CCL20 levels by ELISA. HEK293 and MCC13 cells transfected with a plasmid expressing enhanced GFP (EGFP)-ST or empty vector control were treated with 10 ng/ml TNF-α, and supernatants were collected 24 h posttreatment. Levels of secreted interleukin-8 (IL-8) and CCL20 were detected by enzyme-linked immunosorbent assay (ELISA) using the manufacturer's protocol (R&D Systems).

Luciferase reporter assays. i293-ST and MCC13 cells were transfected with 50 ng of reporter plasmid expressing firefly luciferase under the control of the NF-κB elements from the concanavalin A promoter (32), a cyclic AMP responsive promoter (pCRE), or a tandem AP-1 element reporter using polyethyleneimine (PEI) (Polysciences Inc.) (33). Where appropriate, cells were cotransfected with 1 μg of MCPyV ST expression plasmid or cellular protein (0.5 μg) (e.g., MyD88). Empty plasmid was

added to ensure each transfection received the same amount of total DNA. To normalize for transfection efficiency, 10 ng pRLTK Renilla luciferase reporter plasmid was added to each transfection. Where necessary, at 24 h posttransfection, cells were treated with 10 ng/ml TNF-α, 50 ng/ml tetradecanoyl phorbol acetate (TPA), or 20 ng/ml IL-1α for a further 12 h. Samples were lysed in passive lysis buffer, and activity was measured using a dual luciferase reporter assay (Promega), as previously described (34).

Coimmunoprecipitation assays. Assays were performed as previous described (35, 36). For GST pulldown screens, 293 cells were cotransfected with 1.5 μg of EGFP or EGFP-ST and various GST-tagged expression vectors (described in reference 32) using Lipofectamine 2000. After 24 h, cells were lysed in RIPA buffer, and lysates were bound to glutathione-Sepharose 4B beads (GE Healthcare) for 2 h at 4°C. Beads were washed and then analyzed by immunoblotting using GST- or GFP-specific monoclonal antibodies (Sigma and Living Colors, respectively).

To perform epitope tag-based coimmunoprecipitation assays, 293 cells were transfected with the appropriate vectors. Cellular lysates were harvested after 48 h and then incubated with protein A-agarose beads, GFP-TRAP A beads (Chromotek), anti-FLAG M1 affinity gel (Sigma-Aldrich), or EE-specific antibody (Abcam) bound to protein A-agarose beads for 2 h at 4°C before being washed in phosphate-buffered saline (PBS). Beads were resuspended and analyzed by immunoblotting with the appropriate antibodies.

Endogenous coimmunoprecipitations were performed using uninduced or induced i293-ST cells. After 48 h of induction, precleared cellular lysates were then incubated with no antibody, a control antibody, or a NEMO-specific polyclonal antibody (Abcam) for 2 h prior to addition of protein A-agarose beads, as previously described (37). After an additional 2 h of incubation, beads were washed, and precipitated proteins were analyzed by immunoblotting with a FLAG-specific antibody.

Immunofluorescence. 293, Huh7, and MCC13 cells grown on glass coverslips were transfected with EGFP or EGFP-ST expression vectors. After 24 h, cells were then fixed with 4% paraformaldehyde, permeabilized in 1% Triton X-100, and blocked in PBS-1% bovine serum albumin (BSA) for 1 h. Cells were labeled with the appropriate primary antibodies and then incubated with the appropriate Alexa Fluor-conjugated secondary antibody, as previously described (38, 39). Cells were viewed on a Zeiss 510 meta laser scanning confocal microscope under a 63× oil immersion objective lens, and images were analyzed using the LSM imaging software (Zeiss).

Inhibition of autophagy assay. 293 cells were transfected with 2 μg of pEGFP-cI or pEGFP-ST. After 12 h, the appropriate wells were either mock treated or treated with either an inhibitor cocktail (pepstatin [100 μM] and leupeptin [3.64 μM]) or 3-methyladenine (5 nM) for 12 h at 37°C. Cell lysates were analyzed by immunoblotting using the appropriate antibodies.

SILAC-based immunoprecipitations. iST-293 and i293-FLAG cells were grown in R_0K_0 DMEM containing ^{12}C L-arginine and ^{12}C L-lysine ("light" DMEM) and R_6K_4 DMEM containing ^{13}C L-arginine and ^{13}C L-lysine ("heavy" DMEM), respectively. All stable isotope labeling by amino acids in cell culture (SILAC)-based media was supplied by Dundee Cell Products and supplemented with 10% dialyzed fetal calf serum (Dundee Cell Products). iST-293 and i293-FLAG cells were then induced for 48 h, and cells were lysed in 5 ml ice-cold RIPA buffer. Cellular lysates were then incubated with anti-FLAG M1 affinity gel (Sigma-Aldrich) for 2 h at 4°C, before being washed in PBS. For each sample, beads were resuspended in 40 μl 2× protein solubilizing buffer [50 mM Tris-HCl (pH 6.8), 2% (wt/vol) SDS, 20% (vol/vol) glycerol, 50 μg/ml bromophenol blue, 10 mM dithiothreitol (DTT)] and boiled at 95°C for 5 min, and each amount of samples was then mixed, separated by one-dimensional SDS-PAGE (4 to 12% Bis-Tris Novex minigel; Invitrogen), and visualized by colloidal Coomassie blue staining (Novex; Invitrogen). The entire protein gel lane was excised and cut into 6 gel slices. Each gel slice was then subjected to in-gel digestion with trypsin, and liquid chromatography-tandem mass spectrometry (LC-MS/MS) analysis (University of Bristol Proteomics Facility) was used to identify and quantify the precipitated proteins as previously described (40, 41).

NF-κB pathway activation. i293-ST cells were induced for 42 h and then incubated with serum-free DMEM for 6 h to eliminate nonspecific activation of the NF-κB pathway. Cells were then incubated with 100 ng/ml TNF-α (InvivoGen) in 10% DMEM. Cell lysis was performed in PBS-1% Triton X-100, and lysates were separated into nuclear and cytoplasmic fractions as previously described (42). Proteins were then subjected to immunoblotting, using appropriate antibodies.

RESULTS

MCPyV ST regulates transcription of cellular genes associated with innate immunity. Polyomavirus ST have important functions in viral replication and transformation (10, 11). To analyze the putative functions of MCPyV ST, expression profiling analysis was performed using a Flp-In 293 cell line capable of inducible MCPyV ST expression, termed i293-ST (Fig. 1Ai). The MCPyV ST coding region was initially PCR amplified from genomic DNA isolated from an MCC tumor, incorporating a carboxy-terminal FLAG tag. Sequencing analysis showed that the MCPyV ST gene amplified is identical to the MCC350 isolate (5), with the exception of 3 single nucleotide polymorphisms, none of which result in amino acid changes (data not shown).

Quantitative reverse transcription-PCR arrays were performed using cDNA reversely transcribed from RNA isolated from uninduced or induced i293-ST cells. MCPyV ST expression resulted in a marked downregulation of genes associated with the immune response, in particular markers of innate immunity, such as CCL20, CXCL-9, IL-8, and TANK (Fig. 1Aii). A clear trend of the genes affected shows that many are associated with the NF-κB pathway, either involved in the activation of NF-κB or targeted by NF-κB-specific transcriptional activation (Fig. 1Aii, green or red, respectively).

To independently confirm these findings with regard to MCC, we initially assessed the effect of MCPyV ST expression on innate immune expression markers in the MCPyV-negative MCC13 cell line. MCC13 cells were transfected with either control EGFP or EGFP-ST expression constructs (50 to 60% transfection rate) and then stimulated NF-κB activation using TNF-α. ELISAs were then performed, measuring secreted levels of CCL20 and IL-8. Results showed that in TNF-α-stimulated cells, levels of both CCL20 and IL-8 were downregulated significantly in the presence of MCPyV ST (Fig. 1B). To confirm that the EGFP-ST expression construct was functional, we assessed its ability to stimulate expression from the MCPyV early promoter, as previously shown by other polyomavirus ST (9). Results demonstrate that upon EGFP-ST expression, MCPyV early promoter activity was upregulated almost 3-fold compared to the pEGFP-cI-transfected control, demonstrating that the EGFP-ST fusion protein was functional. Moreover, similar results were also observed in induced i293-ST cells (Fig. 1Biii). Moreover, we also assessed total levels of IκB, as an indicator of NF-κB activation, in MCPyV-negative (MCC13) and MCPyV-positive (MKL-1) MCC cell lines. Immunoblot analysis was performed on MCC13 and MKL-1 cells using an IκB-specific antibody, and densitometry-based quantification demonstrated a reduction of approximately 60% in IκB levels in the MCPyV-positive MKL-1 cell line (Fig. 1C). Together, these data support the expression profiling, confirming that MCPyV ST downregulates NF-κB-targeted transcription.

MCPyV ST regulates NF-κB signaling downstream from receptor complexes. We next determined whether MCPyV ST spe-

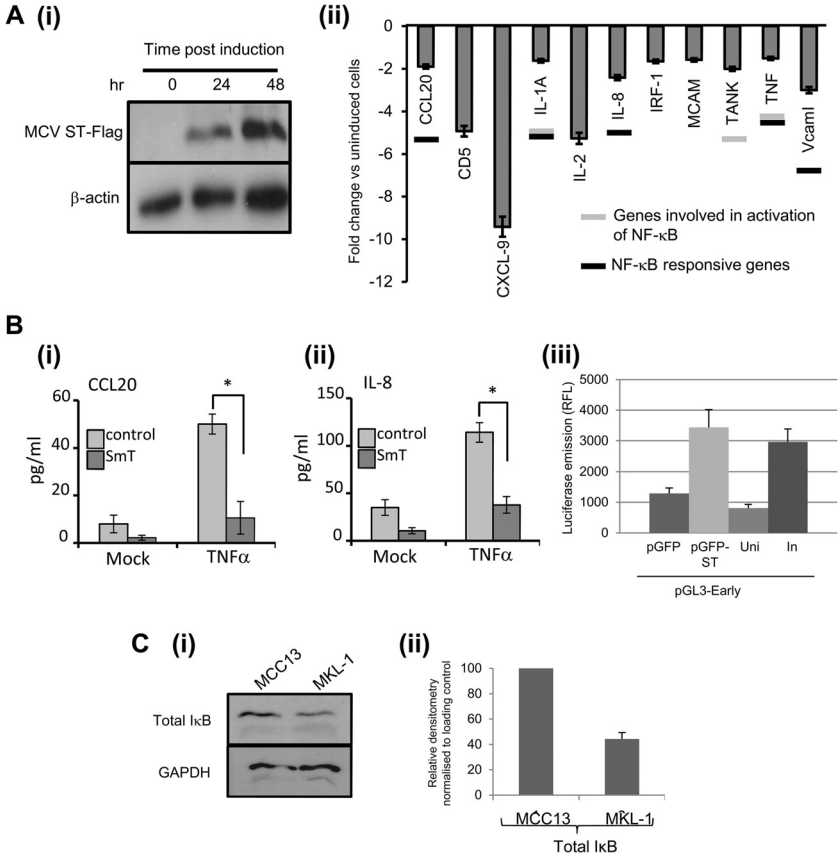

FIG 1 MCPyV ST downregulates cellular gene expression associated with the NF-κB pathway. (A) (i) The MCPyV ST coding region was PCR amplified, incorporating a C-terminal FLAG tag from an MCC tumor, and inserted into pCDNA5/frt/To to yield iST-FLAG. A stable inducible cell line was subsequently produced via site-specific DNA recombination within a Flp-In 293 cell line, termed i293-ST. To verify correct inducible expression of the MCPyV ST fusion protein, i293-ST cells remained uninduced or were incubated for either 24 or 48 h in the presence of doxycycline hyclate. After induction, cell lysates were analyzed by immunoblotting using a FLAG-specific antibody. (ii) RNA was extracted from uninduced or induced i293-ST cells prior to expression profiling using SA Biosciences RT^2 Profiler PCR array systems. Fold changes were calculated using the manufacturer's software. (B) (i) The MCC13 cell line was transfected with plasmids expressing EGFP or EGFP-ST. The cells were treated with TNF-α for 24 h, and levels of secreted IL-8 (i) and CCL20 (ii) were analyzed by ELISA (*, $P < 0.05$ versus control [t test]). (iii) HEK 293 cells were transiently transfected with either pEGFP-cI or pEGFP-ST and pGL3-Early. In addition, uninduced (Uni) or induced (In) i293-ST cells were transfected with pGL3-Early. Cell lysates were harvested after 24 h and used in a luciferase assay to determine the amount of light emitted in relative fluorescence units (RFL). Results show the average luciferase emissions of triplicate measurements. SmT, small T. (C) (i) Cellular lysates from MCC13 (MCPyV negative) and MKL-1 (MCPyV positive) were analyzed by immunoblotting using a total IκB-specific antibody. GAPDH was used as a measure of equal loading. (ii) Densitometry quantification of the Western blots was carried out using ImageJ software and is shown as a percentage of relative densitometry normalized to the loading control GAPDH ($n = 3$).

cifically regulates NF-κB activity and, if so, which part of the pathway is targeted. First, to analyze the effect of MCPyV ST on NF-κB-mediated transcription, expression of a luciferase reporter gene driven by NF-κB was monitored after stimulation of the NF-κB pathway, in the absence or presence of MCPyV ST. Independent experiments were performed in the i293-ST cell and the MCC MCPyV-negative MCC13 cell line transfected with control EGFP or EGFP-ST expression constructs. In both the induced and EGFP-ST-transfected MCC13 cell lines, MCPyV ST expression strongly inhibited NF-κB-driven luciferase expression in response to known NF-κB activating agents, TNF-α, TPA, and IL-1α (Fig. 2A). In contrast, MCPyV ST had no inhibitory effects on TPA-stimulated cyclic AMP (cAMP) response element (CRE) or activating protein 1 (AP-1)-responsive reporter constructs (Fig. 2B). These results indicate that the inhibitory effect of MCPyV ST is specific to the NF-κB pathway.

To initially investigate the possible molecular mechanism of MCPyV ST-mediated inhibition, upstream components of the NF-κB pathway were overexpressed in control versus MCPyV ST-expressing i293-ST and MCPyV-negative MCC13 cells, and NF-κB-driven luciferase expression was measured. In both cell lines, MCPyV ST significantly reduced NF-κB-driven luciferase in response to overexpressed Toll-like receptor (TLR) adaptor proteins MyD88 and TRIF and the ubiquitin ligases TRAF2 and TRAF6 (Fig. 2C). These data suggest that MCPyV ST subverts NF-κB signaling downstream from receptor complexes.

MCPyV ST interacts with NEMO. Our results indicate that MCPyV ST prevents NF-κB activation by a mechanism independent of activated receptor complexes. A plausible alternative is that MCPyV ST interacts with another target protein within the pathway. Therefore, to identify this binding partner, 293 cells were cotransfected with EGFP or EGFP-ST and various GST-tagged proteins, including kinases (MEKK3), inhibitors (Abin2), or regulatory proteins (NEMO) associated with the NF-κB pathway,

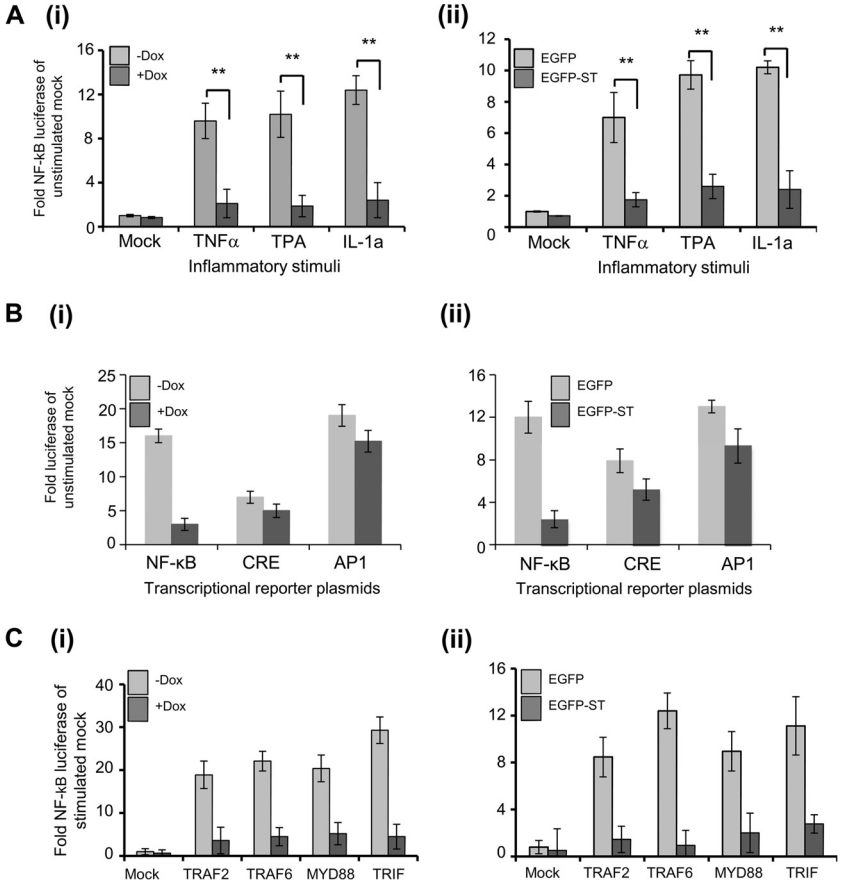

FIG 2 MCPyV ST specifically downregulates NF-κB activity, downstream of receptor complexes. (A) Uninduced or induced i293-ST (i) or MCC13 cells expressing EGFP or EGFP-ST (ii) were transfected with a reporter plasmid expressing firefly luciferase under the control of the NF-κB elements from the concanavalin A promoter. At 24 h posttransfection, cells were treated with 10 ng/ml TNF-α, 50 ng/ml TPA, or 20 ng/ml IL-1α for 12 h. Samples were then analyzed for luciferase activity. To normalize transfection efficiency, 10 ng pRLTK Renilla luciferase reporter plasmid was used. Dox, doxycycline. (B) Cotransfections were performed as described above, using NF-κB, the cyclic-AMP responsive promoter, and tandem AP-1 responsive reporter plasmids, and samples were analyzed for luciferase activity. (C) Uninduced or induced i293-ST (i) or MCC13 cells expressing EGFP or EGFP-ST (ii) were cotransfected with a concanavalin A promoter reporter plasmid and plasmids of the indicated cellular proteins (1 μg of each), and samples were analyzed for luciferase activity, *, $P < 0.05$ versus control (*t* test).

and coimmunoprecipitations were performed using GST-Sepharose 4B beads. Results show enhanced binding between MCPyV ST and the GST-tagged NF-κB essential modulator (NEMO); in contrast, no other interactions were observed with other tagged proteins associated with the NF-κB pathway (Fig. 3A). To confirm the interaction observed between MCPyV ST and NEMO, a series of additional coimmunoprecipitations were performed. Cell lysates expressing EGFP or EGFP-ST and either GST or GST-tagged NEMO were incubated with protein A-agarose beads alone or conjugated with a control or GFP-specific antibodies. Results show that MCPyV ST interacted with NEMO (Fig. 3B). To address potential overexpression artifacts, coimmunoprecipitations were also performed in uninduced versus induced i293-ST cells using a NEMO-specific antibody. Immunoblot analysis using a FLAG-specific antibody also showed a weak but consistent interaction between MCPyV ST and endogenous NEMO (Fig. 3C).

We next determined whether MCPyV ST colocalized with NEMO. The MCPyV-negative MCC cell line, MCC13, and Huh7 cells were transfected with plasmids expressing either EGFP or EGFP-ST, in the presence of a NEMO-myc expression vector, and colocalization was visualized by direct GFP fluorescence (Fig. 4A and B). Huh7 cells were utilized instead of 293 cells in this experiment to allow clear visualization of cytoplasmic structures. Results from both cell lines show the subcellular localization of NEMO in EGFP-expressing cells residing throughout the cytoplasm and nucleus, with small discrete foci present in both compartments as previously described (43). In contrast, expression of EGFP-ST resulted in an increase in the number and size of the cytoplasmic puncta, which exhibited significant colocalization of NEMO with a proportion of MCPyV ST. This was particularly evident in the EGFP-ST-transfected MCC13 cell line. In addition, confocal imaging suggests that the puncta are cytoplasmic, but we cannot rule out the presence of some nuclear puncta. Together, these data provide the first evidence of an interaction between MCPyV ST and NEMO.

MCPyV ST does not promote the degradation of NEMO. The distinct cytoplasmic puncta containing NEMO and MCPyV ST are reminiscent of autophagosomes (44). Interestingly, human cytomegalovirus (HCMV) targets NEMO for autophagosomal degradation, curtailing the cellular inflammatory response (26). To investigate whether MCPyV ST targets NEMO to autophagosomes for degradation, we assessed whether the cytoplasmic

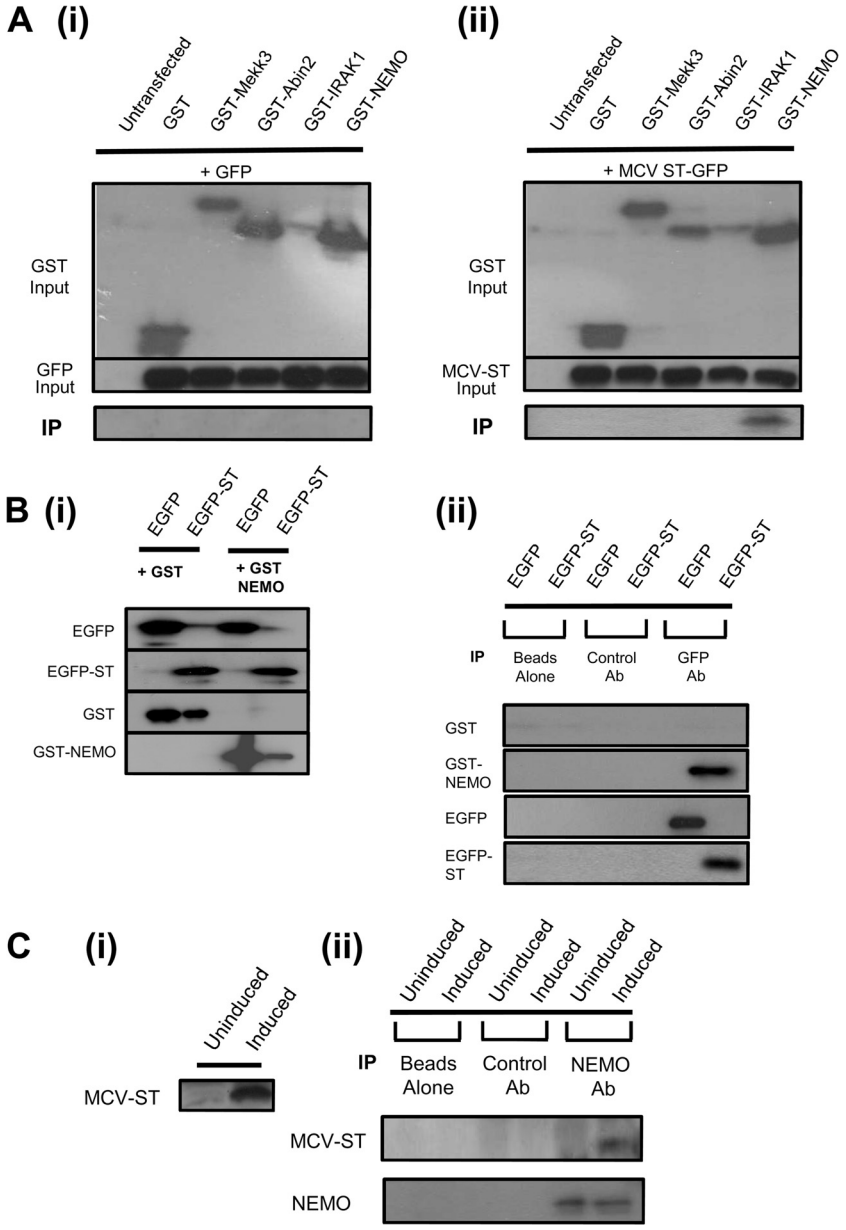

FIG 3 MCPyV ST interacts with NEMO. (A) 293 cells were cotransfected with either EGFP or EGFP-ST and the indicated GST-tagged eukaryotic expression vectors. After 24 h, cell lysates were incubated with GST-Sepharose 4B beads, and interacting proteins were immunoblotted with GFP-specific antibodies. (B) 293 cells were cotransfected with EGFP or EGFP-ST in the presence of either GST or GST-NEMO expression vectors. (i) Transfected cell lysates were probed with GFP-, FLAG-, and GST-specific antibodies to serve as a loading control (inputs). (ii) Transfected cell lysates were then incubated with either beads alone control, control antibody (Ab), or GFP-TRAP affinity beads, and bound protein was immunoblotted with a GST-specific antibody in addition to a GFP-specific antibody as a precipitation control. (C) (i) i293-ST cells remained uninduced or were incubated with doxycycline for 48 h. Cellular lysates were immunoblotted with a FLAG-specific antibody. (ii) Cellular lysates were then incubated with polyclonal NEMO-specific antibody bound to protein A-Sepharose beads, and precipitated proteins were then immunoblotted with a FLAG-specific antibody in addition to monoclonal NEMO-specific antibody as a precipitation control.

puncta containing MCPyV ST and NEMO observed colocalized with the autophagosome marker, microtubule-associated protein 1A/1B-light chain 3 (LC3) (45). Figure 4C shows that LC3 was observed in cytoplasmic foci, distinct from the foci containing MCPyV ST and NEMO.

Endogenous NEMO levels were also assessed in the presence of MCPyV ST. 293 cells expressing EGFP or EGFP-ST were left untreated or incubated for 12 h with an autophagy inhibitor, a lysosomal protease inhibitor (PI) mixture, or 3-methyladenine (3-MA). Results show that endogenous NEMO levels remained unchanged in the presence of EGFP or MCPyV ST. Moreover, no discernible changes in NEMO levels were observed after the addition of autophagy inhibitors (Fig. 4D). To confirm the functionality of the autophagy inhibitor 3-MA, Beclin1 levels were assessed. 3-MA reduced the levels of Beclin1 back to untreated levels in the presence of the autophagy inducer rapamycin (data not shown). Together, these results indicate that NEMO is not targeted to autophagosomes nor degraded by MCPyV ST.

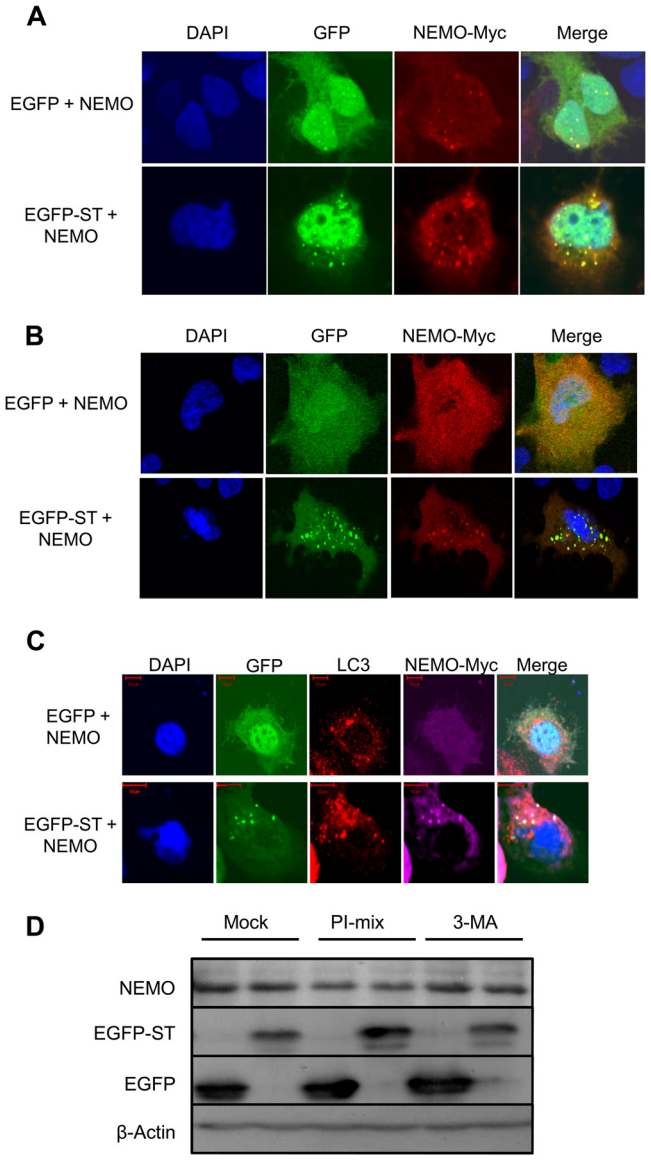

FIG 4 A proportion of MCPyV ST colocalizes with NEMO. Following transfection of Huh7 (A) and MCC13 (B) cells with either pEGFP or pEGFP-ST in the presence of pNEMO-myc, after 24 h, cells were fixed and permeabilized, and GFP fluorescence was analyzed by direct visualization, whereas NEMO was identified by indirect immunofluorescence using a Myc-specific antibody. (C) A similar experiment was repeated, but Huh7 cells were stained with LC3- and Myc-specific antibodies. (D) 293 cells were transfected with pEGFP-cI or pEGFP-ST. After 12 h, the appropriate wells were either mock treated or treated with either a protease inhibitor (PI) cocktail or 3-methyladenine for 12 h. Cell lysates were then analyzed by immunoblotting using the indicated antibodies. DAPI, 4′,6-diamidino-2-phenylindole.

MCPyV ST prevents phosphorylation of IκB and inhibits nuclear translocation of NF-κB. After demonstrating that MCPyV ST targets NF-κB activity downstream of receptor complexes and establishing that MCPyV ST interacts with but does not degrade NEMO, we speculated that MCPyV ST may inhibit nuclear translocation of NF-κB, resulting in the observed inhibition of NF-κB-dependent transcription. Furthermore, as IκB phosphorylation and subsequent release from NF-κB are mediated by interactions between NEMO and upstream kinases, we also envisaged that the interaction between MCPyV ST and NEMO may interfere with the phosphorylation status of cytoplasmic IκB upon NF-κB stimulation, prolonging IκB binding to NF-κB and rendering it inactive.

The effect of MCPyV ST on NF-κB activation, following TNF-α stimulation, was therefore investigated. i293-ST cells remained uninduced or MCPyV ST expression was induced for 42 h, prior to 6 h serum starvation, to prevent nonspecific activation of the NF-κB pathway; NF-κB activation was then stimulated using TNF-α. Nuclear and cytoplasmic fractions were then subjected to immunoblotting and densitometry-based quantification to analyze p50, RelA, and phosphorylated IκB levels. Phosphorylated IκB was not detected in either the nuclear or cytoplasmic samples from unstimulated cells (Fig. 5A), showing no NF-κB activation in the absence of TNF-α. In contrast, TNF-α-stimulated cells, which remained uninduced, showed high levels of phosphorylated IκB in cytoplasmic fractions. Strikingly, stimulated cells expressing MCPyV ST showed a significant reduction of approximately 60% in cytoplasmic phosphorylated IκB levels. Furthermore, nuclear levels of p50 and RelA were also markedly lower, approximately 50%, in TNF-α-activated cells expressing MCPyV ST, compared with uninduced cells (Fig. 5A and B). This suggests that MCPyV ST inhibits IκB phosphorylation through an interaction with NEMO, reducing the nuclear translocation of NF-κB subunits and subsequent activation of NF-κB responsive genes.

MCPyV ST inhibits IKKα/IKKβ phosphorylation. The IKK complex plays an essential role in NF-κB signaling (21). It phosphorylates inhibitory IκB proteins, resulting in their proteasomal degradation, in turn releasing NF-κB proteins and allowing their nuclear translocation. Activation of the IKK complex depends on phosphorylation of its two catalytic subunits, IKKα and IKKβ. Having demonstrated that MCPyV ST interacts with the IKK component NEMO, and also affects the phosphorylation status of IκB, we next assessed the phosphorylation status of IKKα and IKKβ in uninduced and MCPyV ST-expressing cells upon TNF-α stimulation. Treatment with TNF-α led to a rapid but transient increase in IKKα/IKKβ phosphorylation (Ser176/177) (Fig. 6A), returning to basal levels by 60 min in uninduced cells. In contrast, MCPyV ST expression led to a marked reduction in IKKα/IKKβ phosphorylation levels (Fig. 6A). Densitometry-based quantification shows this reduction is between 60 and 70% in the presence of MCPyV ST (Fig. 6B). Importantly, cells treated with the broad-spectrum phosphatase inhibitor okadaic acid increased IKKα/IKKβ phosphorylation in MCPyV ST-expressing cells, suggesting cellular phosphatases are involved in MCPyV ST-mediated regulation of the IKK complex.

SILAC-based immunoprecipitations identify PP4C and PP2A Aβ as novel MCPyV ST binding partners. Having established that MCPyV ST expression results in a marked reduction in phosphorylated IKKα and IKKβ levels, and that this reduction can be inhibited using the broad-spectrum phosphatase inhibitor okadaic acid, the interaction with MCPyV ST and cellular phosphatases was further examined. Polyomavirus ST-PP2A interactions are well characterized (46); however, surprisingly, the interaction between MCPyV ST and PP2A Aα is not required for MCPyV ST-mediated cellular transformation (14). Therefore, SILAC-based pulldown assays were employed to identify additional MCPyV ST cellular phosphatase-interacting partners. This technique facilitates the detection of lower abundance proteins, in

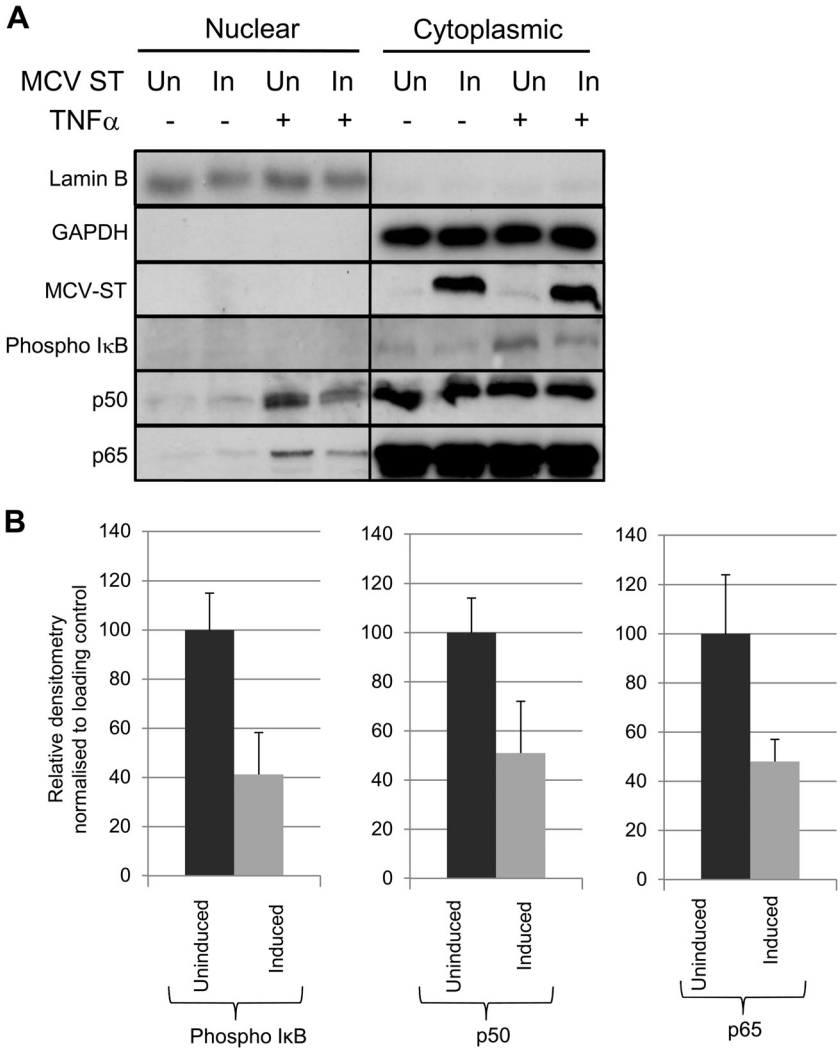

FIG 5 MCPyV ST inhibits phosphorylation of IκB and prevents nuclear translocation of the NF-κB heterodimer. (A) i293-ST cells remained uninduced (Un) or induced (In) for MCPyV ST expression. Cells were then serum starved before TNF-α was used to stimulate activation of the NF-κB pathway. Nuclear and cytoplasmic fractions were then isolated and analyzed by immunoblotting to detect phosphorylation of IκB and levels of nuclear translocation of p65 and p50 using the indicated antibodies. (B) Densitometry quantification of the Western blots was carried out using ImageJ software and is shown as a percentage of relative densitometry normalized to the loading control GAPDH. Standard deviations of 3 replicated experiments are shown.

particular those interacting in substoichiometric amounts or binding with lower affinity in multiprotein complexes (47, 48). i293-ST cells expressing the MCPyV ST-FLAG-tagged protein were metabolically labeled in "heavy" media containing ^{13}C isotopes of arginine and lysine, while FLAG-expressing control cells were grown in "light" media containing the ^{12}C isotopes. Cell lysates were then incubated with FLAG affinity beads, and precipitated proteins were identified by LC-MS/MS analysis. False positives immunoprecipitated with the FLAG control were discounted, allowing true MCPyV ST interacting partners to be identified. MCPyV ST precipitated two additional cellular phosphatase subunits, PP4C and PP2A Aβ (Fig. 7A). PP2A Aα was also precipitated but around 40 times less efficiently than the other subunits. Surprisingly, NEMO was not precipitated in this experiment, but this was probably due to the experiment being performed in unstimulated cells. Moreover, the interaction between NEMO and MCPyV ST may be transient and not direct, which reduces its potential to be identified in this experiment.

To verify the putative interactions between MCPyV ST and the cellular phosphatases, coimmunoprecipitations were performed in 293 cells transfected with either EGFP or EGFP-ST in the presence of control, FLAG-PP4C, or EE-PP2A Aβ expression vectors. For PP4C immunoprecipitations, cell lysates were incubated with protein A-agarose beads alone or conjugated with a control or FLAG-specific antibodies, and precipitated proteins were identified using a GFP-specific antibody. For PP2A Aβ, cell lysates were incubated with GFP-TRAP beads, and immunoprecipitated proteins were identified using an EE-specific antibody. Results show that MCPyV ST interacts with both PP4C and PP2A Aβ subunits (Fig. 7B and C).

To elucidate whether MCPyV ST expression leads to the redistribution of PP4C or PP2A Aβ subunits into the cytoplasmic puncta associated with NEMO, FLAG-PP4C or EE-PP2A Aβ was expressed in Huh7 cells expressing either EGFP or EGFP-ST and NEMO-Myc. Results demonstrate that in the presence of MCPyV ST, PP4C is present in the puncta containing NEMO; in contrast,

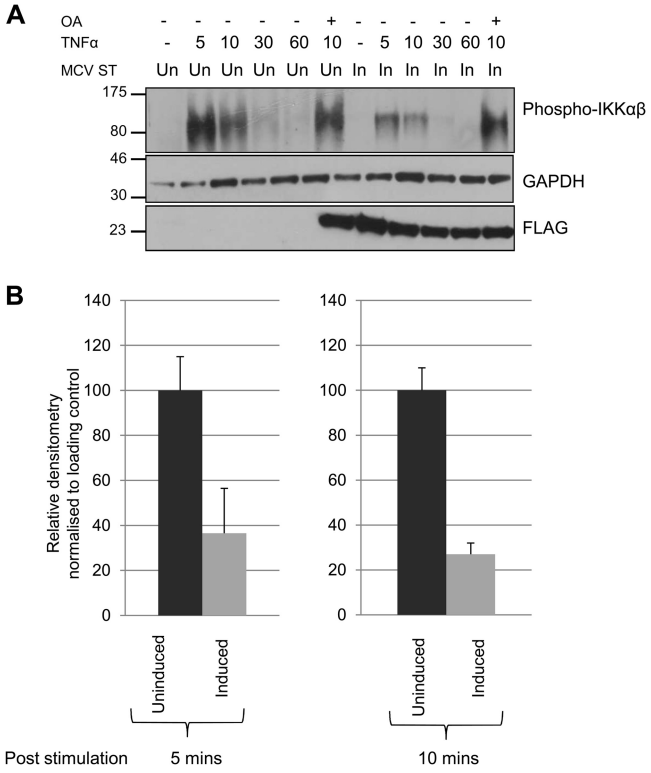

FIG 6 Cellular phosphatases are required to inhibit IKKα/IKKβ phosphorylation. (A) i293-ST cells remained uninduced or induced for MCPyV ST expression. Cells were then serum starved before TNF-α was used to stimulate activation of the NF-κB pathway. Cells were lysed directly into SDS sample buffer, and lysates were immunoblotted to detect phosphorylation of IKKα/IKKβ (Ser176/177). GAPDH was used as a loading control, and FLAG blotting detected expression of MCPyV ST. OA, okadaic acid. (B) Densitometry quantification of the Western blots at 5 and 10 min time points was carried out using ImageJ software and is shown as a percentage of relative densitometry normalized to the loading control GAPDH. Standard deviations of 3 replicated experiments are shown.

no colocalization is observed in EGFP control cells (Fig. 8A). However, it is difficult to draw the same conclusion regarding PP2A Aβ, as there is a colocalization between PP2A Aβ and NEMO in control cells, although MCPyV ST does colocalize with PP2A Aβ and NEMO (Fig. 8B). This suggests that MCPyV ST may manipulate cellular phosphatases to modulate the NF-κB pathway.

To determine whether an enhanced interaction is observed between NEMO and the cellular phosphatases in the presence of MCPyV ST, coimmunoprecipitation assays were performed. 293 cells were transfected with either EGFP or EGFP-ST in the presence of NEMO-Myc, in addition to either an empty FLAG or EE control vector or a FLAG-PP4C or EE-PP2A Aβ expression vector. Cell lysates were then incubated with a polyclonal Myc-specific antibody to precipitate NEMO, and the amount of EGFP, EGFP-ST, or cellular phosphatase proteins also precipitated was identified using GFP-, FLAG-, and EE-specific antibodies. Results show that in the presence of EGFP-ST, an increase in precipitated FLAG-PP4C or EE-PP2A Aβ is observed compared with the presence of control EGFP alone. Moreover, an increase in precipitated EGFP-ST is also observed in the presence of both cellular phosphatases, particularly PP4C (Fig. 8C). This suggests that MCPyV ST can enhance the interaction between the cellular phosphatases and NEMO.

An interaction between MCPyV ST, NEMO, and the cellular phosphatase subunits PP4C and/or PP2A Aβ, but not PP2A Aα, is required for MCPyV ST-mediated downregulation of NF-κB-targeted transcription. To identify the domains within MCPyV ST which are required for the interaction between NEMO and the cellular phosphatase PP4C, a carboxy-terminal truncation series of MCPyV ST was produced (Fig. 9A). In addition, the site-directed mutant of MCPyV ST, R7A, was utilized, which has previously been reported to abolish the interaction between MCPyV ST and PP2A Aα (14). Coimmunoprecipitation assays were then performed with each truncation and R7A mutant. Initially, 293 cells were transfected with an EGFP control vector, EGFP-ST, the EGFP-R7A mutant, or each EGFP carboxy-terminal truncation in the presence of a FLAG-PP4C expression vector. Cell lysates were then incubated with FLAG affinity resin to precipitate FLAG-PPC4, and Western blot analysis was performed using a GFP-specific antibody to assess the presence of interacting GFP-ST fusion proteins. Results show that the R7A mutant, which inhibited the interaction between MCPyV ST and PP2A Aα, still associated with PP4C. However, analysis of the MCPyV ST carboxy-terminal truncation series showed that a region containing residues 95 to 128 is required for PP4C binding (Fig. 9B). A similar experiment was also performed to map the MCPyV ST interaction domain required for NEMO binding. 293 cells were transfected with an EGFP control vector, EGFP-ST, the EGFP-R7A mutant, or each EGFP carboxy-terminal truncation in the presence of a NEMO-myc expression vector. Cell lysates were then incubated with GFP-TRAP affinity beads, and Western blot analysis was performed using a Myc-specific antibody to assess the precipitation of NEMO-myc. Results again showed that the R7A mutant was still able to interact with NEMO, suggesting that an interaction with PP2A Aα is not required for the interaction between NEMO and MCPyV ST. In contrast, deletion of residues 95 to 128 abolished the interaction with NEMO (Fig. 9C). Together, these data suggest that the interaction between MCPyV ST, NEMO, and PP4C requires residues 95 to 128 within MCPyV ST, although it must be noted that these large-scale truncations of MCPyV ST may affect other functions of the ST protein. Moreover, it also suggests that PP2A Aα is not required for the interaction between NEMO or PP4C and MCPyV ST.

To analyze the functional significance of residues 95 to 128 of MCPyV ST in more detail, two further internal deletion mutants were produced. These specifically deleted either residues 95 to 111 or residues 111 to 128 within the MCPyV ST protein but retained the carboxy terminus (Fig. 10A). Similar coimmunoprecipitation analyses were performed as described for the carboxy truncation mutants above (Fig. 10B and C). Results showed that deletion of residues 111 to 128 (Δ111-128 mutant) had no effect on NEMO or PP4C binding. However, residues 95 to 128 of MCPyV ST are required for the interaction between MCPyV ST and both NEMO and PP4C. Moreover, we also assessed the ability of the R7A, Δ95-111, and Δ111-128 mutants to interact with PP2A Aβ (Fig. 10D). Cell lysates were incubated with GFP-TRAP beads, and immunoprecipitated proteins were identified using an EE-specific antibody. Results showed that wild-type MCPyV ST and the R7A mutant interacted with PP2A Aβ, but residues 95 to 111 are also required for the interaction between MCPyV ST and PP2A Aβ. Together, these data suggest that residues 95 to 111 are required

A

Protein name	Gene name	Light: heavy ratio	Peptide hits
PP2A A subunit β isoform	PPP2R1B	100.00	11
PP4C	PPP4C	100.00	7
PP2A A subunit α isoform	PPP2R1A	2.47	16

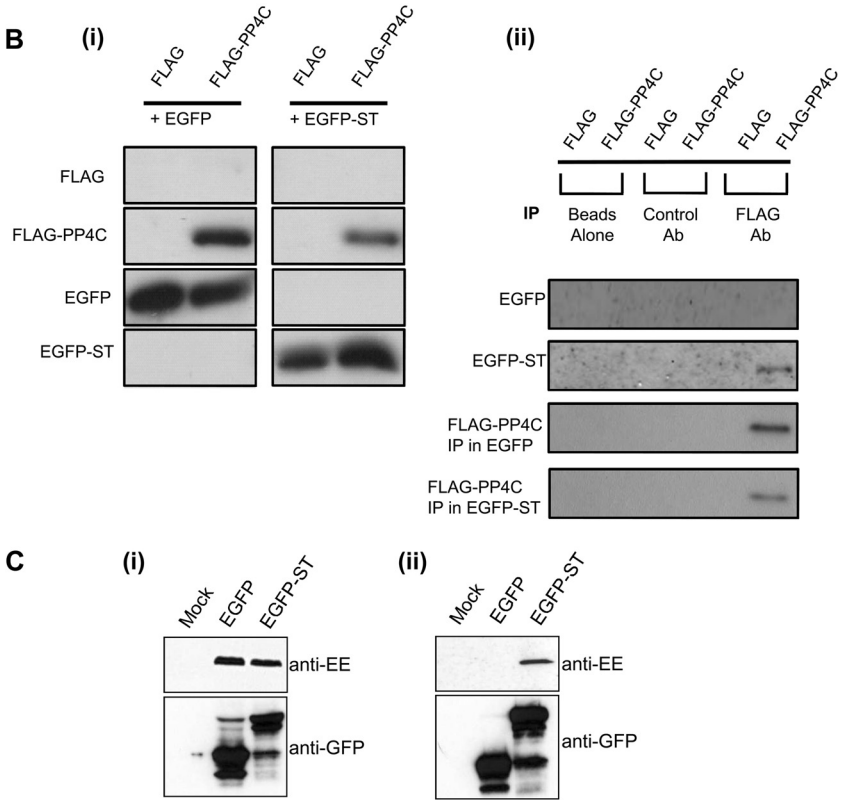

FIG 7 MCPyV ST interacts with cellular phosphatase subunits PP4C and PP2A Aβ. (A) iST-293 and i293-FLAG cells were grown in "light" and "heavy" DMEM, respectively. Induced cellular lysates were then incubated with anti-Flag M1 affinity gel, and precipitated proteins were separated by one-dimensional SDS-PAGE. LC-MS/MS analysis was then performed to identify precipitated proteins. (B) 293 cells were cotransfected with EGFP or EGFP-ST in the presence of either control or FLAG-PP4C expression vectors. (i) Transfected cell lysates were probed with GFP- and FLAG-specific antibodies to serve as a loading control (Input). (ii) Transfected cell lysates were then incubated with either beads alone control, control antibody, or FLAG affinity gel, and bound protein was immunoblotted with a GFP-specific antibody in addition to FLAG-specific antibody as a precipitation control. (C) 293 cells remained untransfected or were cotransfected with EGFP or EGFP-ST in the presence of an EE-PP2A Aβ expression vector. (i) Transfected cell lysates were probed with GFP- and EE-specific antibodies to serve as a loading control (Input). (ii) Transfected cell lysates were then incubated with GFP-TRAP affinity beads, and bound protein was immunoblotted with an EE-specific antibody.

for the interaction between MCPyV ST, NEMO, and the cellular phosphatase subunits PP4C and PP2A Aβ.

Importantly, to confirm that the Δ95-111 and Δ111-128 mutants retained other MCPyV ST functions, we assessed their ability to stimulate expression from the MCPyV early promoter, as previously shown in Fig. 1Biii. Results demonstrate that both mutants upregulated the MCPyV early promoter almost 3-fold, similar to wild-type ST, compared with the pEGFP-cI-transfected control (Fig. 10E). This demonstrates that the Δ95-111 and Δ111-128 mutants do retain other MCPyV ST functions.

We next determined the effect of the MCPyV ST Δ95-111- and Δ111-128-specific deletions and the R7A mutant on the ability of MCPyV ST to downregulate NF-κB-targeted transcription. To this end, expression of the luciferase reporter gene driven by NF-κB was monitored after stimulation of the NF-κB pathway, in the absence or presence of control EGFP, EGFP-ST, EGFP-ST R7A, EGFP-ST Δ95-111, and Δ111-128 mutants (Fig. 10F). As previously described, MCPyV ST expression strongly inhibited NF-κB-driven luciferase expression in response to TNF-α. A similar inhibition was observed for the R7A mutant, which suggests that PP2A Aα is not required for MCPyV ST-mediated downregulation of NF-κB-targeted transcription. In contrast, analysis of MCPyV ST Δ95-111 and Δ111-128 demonstrated that the Δ95-111 mutant, which failed to interact with PP4C and PP2A Aβ and NEMO, was unable to downregulate NF-κB-targeted transcription. This suggests that the interaction between the cellular phosphatases PP4C and/or PP2A Aβ, NEMO, and MCPyV ST is required for the MCPyV ST-mediated suppression of NF-κB signaling.

Together, these data suggest that a possible mechanism of

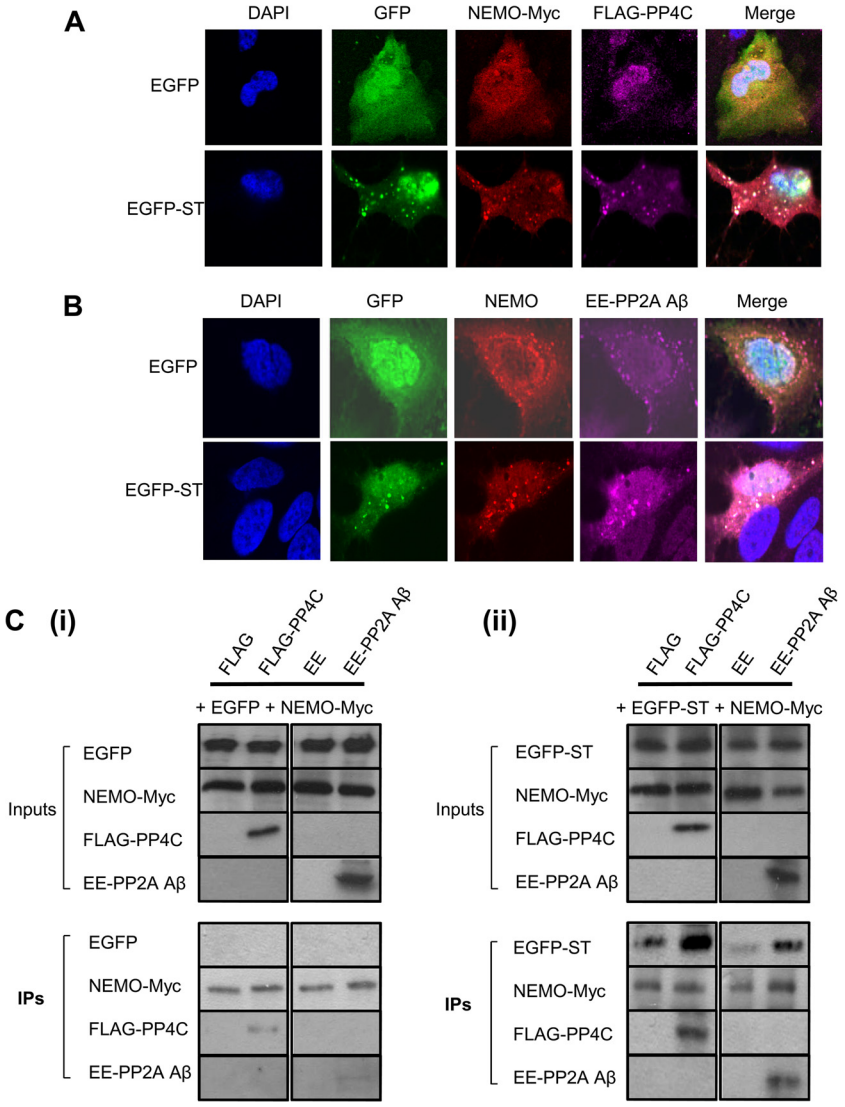

FIG 8 MCPyV ST colocalizes with NEMO and cellular phosphatase subunits PP4C and PP2A Aβ in discrete cytoplasmic puncta. (A) Huh7 cells were transfected with either EGFP or EGFP-ST in the presence of Myc-NEMO and FLAG-PP4C expression vectors. After 24 h, cells were fixed and permeabilized, and GFP fluorescence was analyzed by direct visualization, whereas NEMO and PP4C were identified by indirect immunofluorescence using Myc- and FLAG-specific antibodies, respectively. (B) A similar experiment was repeated, but cells were transfected with either EGFP or EGFP-ST in the presence of EE-PP2A Aβ expression vectors. GFP fluorescence was analyzed by direct visualization, whereas endogenous NEMO and PP2A Aβ were identified by indirect immunofluorescence using NEMO- and EE-specific antibodies, respectively. (C) 293 cells were cotransfected with EGFP (i) or EGFP-ST (ii) in the presence of NEMO-myc and either control or FLAG-PP4C or EE-PP2A Aβ expression vectors. (i) Transfected cell lysates were probed with GFP-, Myc-, FLAG-, or EE-specific antibodies to serve as a loading control (Inputs). Transfected cell lysates were then incubated with Myc affinity gel, and bound protein was immunoblotted with a GFP-, FLAG-, or EE-specific antibody in addition to a NEMO-specific antibody as a precipitation control.

MCPyV ST-mediated NF-κB-targeted transcriptional repression is through the activity of specific cellular phosphatases and that dephosphorylation of the IKK complex may be an important target for this inhibition.

DISCUSSION

Herein we identify MCPyV ST as a novel inhibitor of NF-κB in response to a variety of inflammatory stimuli. This is the first immunomodulatory function ascribed to any polyomavirus ST which may provide protection against the localized immune response during the MCPyV life cycle and MCPyV-mediated tumorigenesis. Through expression profiling, we first demonstrated a general downregulation of NF-κB activation and NF-κB-responsive gene transcription.

Although this downregulation was initially identified using an inducible MCPyV ST expression system based on a 293 cell line, we have also confirmed a downregulation of total levels of IκB in an MCPyV-positive MCC cell line compared with an MCPyV-negative MCC cell line and also downregulation of NF-κB-mediated transcription using 293 and MCC cell lines. Interestingly, these results are supported by digital subtractive data sets identifying cellular genes differentially expressed between MCPyV-positive and MCPyV-negative MCC tumors (49). Although, the article did not focus on the NF-κB pathway, data sets show a similar

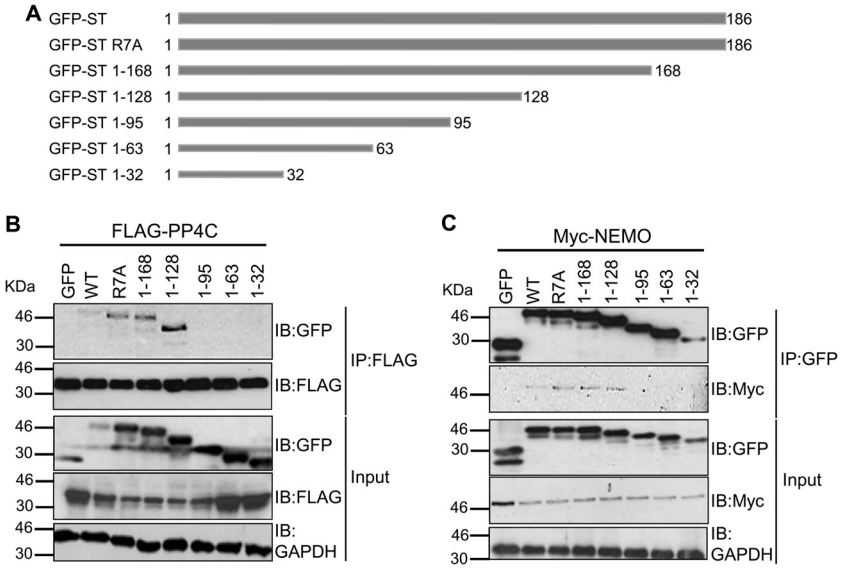

FIG 9 Mapping the domains within MCPyV ST which are required for the interaction with NEMO and PP4C. (A) Schematic representation of the EGFP-tagged MCPyV ST R7A and carboxy-terminal truncation series. (B) 293 cells were cotransfected with either an EGFP control vector, EGFP-ST, EGFP-ST R7A, or each EGFP carboxy-terminal truncation in the presence of a FLAG-PP4C expression vector. Transfected cell lysates were probed with GFP-, FLAG-, or GAPDH-specific antibodies to serve as a loading control (Input). Transfected cell lysates were then incubated with FLAG affinity gel, and bound protein was immunoblotted (IB) with GFP-specific antibodies in addition to FLAG-specific antibody as a precipitation control. (C) 293 cells were cotransfected with either an EGFP control vector, EGFP-ST, EGFP-ST R7A. or each EGFP carboxy-terminal truncation in the presence of a NEMO-myc expression vector. Transfected cell lysates were probed with GFP-, Myc-, or GAPDH-specific antibodies to serve as a loading control (Input). Transfected cell lysates were then incubated with GFP-TRAP affinity gel, and bound protein was immunoblotted with Myc-specific antibodies in addition to GFP-specific antibody as a precipitation control.

downregulation of NF-κB-associated genes, such as NF-κB1A, IL1R1, IKBKB, IRAK1, NF-κB1, and TRAF2. Moreover, these data were also validated by ELISA and reporter gene assays, demonstrating significant downregulation of NF-κB-targeted transcription in the presence of MCPyV ST in both 293 and MCC cell lines.

NF-κB pathway inhibition is a common mechanism used by viruses to subvert the host innate response, preventing expression of cytokines, chemokines, and proteins involved in antigen presentation (22). This aids the establishment of infection and enables virus replication to proceed. Further investigation into the mechanism of MCPyV ST-mediated NF-κB inhibition indicated that MCPyV ST acts downstream of receptor complexes and interacts with NEMO at the IKK complex. This complex is a junction point that integrates signaling from numerous upstream pathways. By inhibiting IKK, it is assumed that MCPyV ST would be able to block signals emanating from endocytic and cytosolic PRRs, in addition to inflammatory receptors, such as TNFR. This represents an effective strategy for immune evasion, where expression of one protein, namely, ST, is able to ablate an immune response to MCPyV infection. Moreover, NEMO controls NF-κB activation in response to a wider range of stimuli. Of particular interest, NEMO is necessary for NF-κB activation in response to DNA damage. As levels of DNA damage are increased during polyomavirus replication (50), it is plausible that ST may also inhibit these signaling events.

NEMO is an attractive target for virus subversion of host responses, and various studies highlight the strategies utilized to inhibit IKK activation. Kaposi's sarcoma-associated herpesvirus (HPV) ORF71 protein binds NEMO, regulating NF-κB both positively and negatively (51). Similarly, HPV E7 protein also inhibits activation of NF-κB by attenuating the IκB complex, although the molecular mechanism is unknown (24). Conversely, human T-cell leukemia virus type 1 (HTLV-1) tax protein also interacts with NEMO, resulting in stimulation of NF-κB signaling (52). Viruses are therefore able to gain advantages by either stimulating or inhibiting the NF-κB pathway. Activation can result in increased cell proliferation, which provides molecular components essential to virus replication.

Our findings suggest that MCPyV ST binds NEMO to negatively regulate NF-κB, helping MCPyV to evade the host antiviral response. MCPyV ST expression prevents phosphorylation of IκBα, rendering NF-κB inactive in the cytoplasm and unable to translocate into the nucleus and activate its transcriptional targets. Specifically, both subunits of the NF-κB heterodimer (p50 and RelA) show a marked decrease in the nucleus when stimulated with TNF-α in the presence of MCPyV ST. The interaction between MCPyV ST and NEMO does not result in NEMO degradation, as observed with HCMV infection (26), but we observed a clear localization of MCPyV ST, NEMO, and the cellular phosphatase PP4C and PP2A Aβ subunits in discrete cytoplasmic puncta. Further analysis suggests that MCPyV ST preferentially interacts with NEMO to prevent IKKα/IKKβ phosphorylation necessary for effective NF-κB activation, and this is dependent on cellular phosphatases. Interestingly, contrary to the progress made in elucidating the mechanisms which regulate the activation of the IKK complex, the processes which regulate deactivation of the IKK complex are poorly understood. To date, only a few cellular phosphatases have been implicated in the regulation and termination of NF-κB activity in a cell-, pathway-, or substrate specific manner (53–55). Of particular relevance, both PP2A and more recently PP4C have been shown to dephosphorylate and inacti-

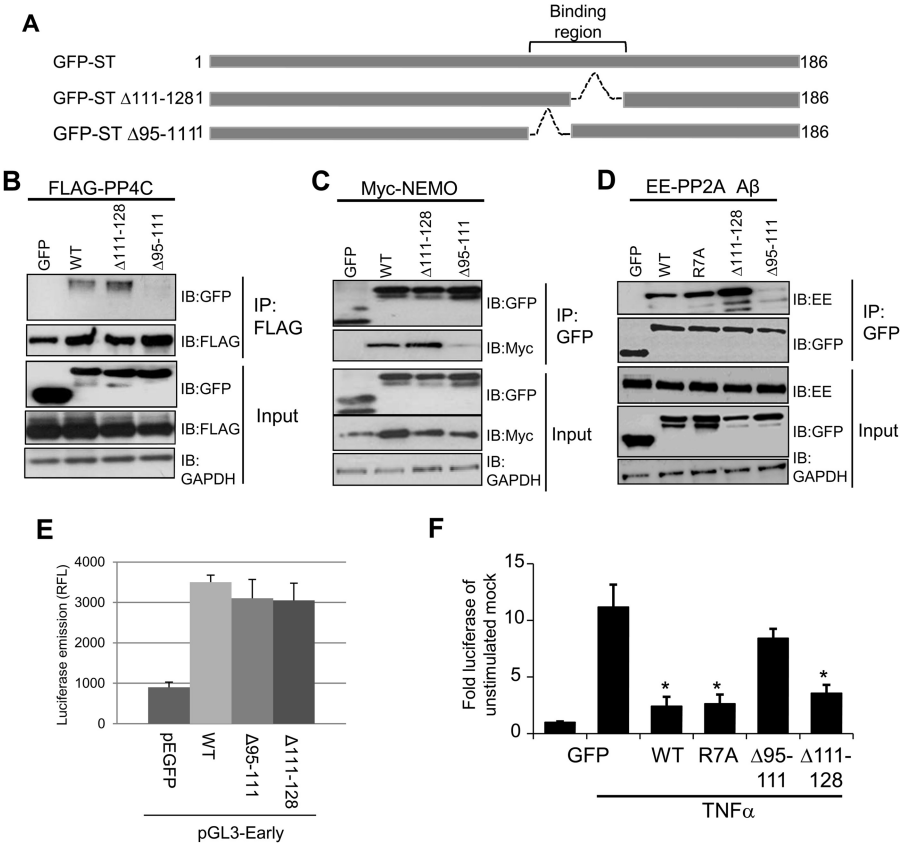

FIG 10 An interaction between MCPyV ST, NEMO, and the cellular phosphatase subunits PP4C and/or PP2A Aβ is required for MCPyV ST-mediated downregulation of NF-κB-targeted transcription. (A) Schematic representation of the EGFP-tagged MCPyV ST internal deletions of residues 95 to 111 and 111 to 128. (B) Coimmunoprecipitation assays were performed as described in the legend to Fig. 9B using 293 cells cotransfected with an EGFP control vector, EGFP-ST, or either the EGFP-STΔ95–111 or Δ111–128 mutant in the presence of a FLAG-PP4C expression vector. WT, wild type. (C) Coimmunoprecipitation assays were performed as described in the legend to Fig. 9C using 293 cells cotransfected with an EGFP control vector, EGFP-ST or either the EGFP-STΔ95–111 or Δ111–128 mutant in the presence of a Myc-NEMO expression vector. (D) Coimmunoprecipitation assays were performed using 293 cells cotransfected with an EGFP control vector, EGFP-ST, or R7A or either the EGFP-STΔ95–111 or Δ111–128 mutant in the presence of an EE-PP2A Aβ expression vector. Transfected cell lysates were probed with EE-, GFP-, or GAPDH-specific antibodies to serve as a loading control (Input). Transfected cell lysates were then incubated with GFP-TRAP affinity gel, and bound protein was immunoblotted with an EE-specific antibody in addition to GFP-specific antibody as a precipitation control. (E) HEK 293 cells were transiently transfected with pEGFPcI, pEGFP-ST, R7A, Δ95–111 mutant, Δ111–128 mutant, or pGL3-Early. Cell lysates were harvested after 24 h and used in a luciferase assay to determine the amount of light emitted in relative fluorescence units (RFL). Results show the average luciferase emissions of triplicate measurements. (F) MCC13 cells expressing EGFP, EGFP-ST, EGFP-ST R7A, EGFP-Δ95–111 mutant, or Δ111–128 mutant were transfected with a reporter plasmid expressing firefly luciferase under the control of the NF-κB elements from the concanavalin A promoter. At 24 h posttransfection, cells were treated with 10 ng/ml TNF-α for 12 h. Samples were then analyzed for luciferase activity. To normalize transfection efficiency, 10 ng pRLTK Renilla luciferase reporter plasmid was used, and values were normalized relative to the densitometry expression levels of the EGFP and EGFP-ST vector signals. *, $P < 0.05$ versus GFP plus TNF-α (*t* test).

vate the IKK complex (55, 56), suggesting that these are ideal cellular phosphatases for MCPyV ST to recruit in order to mediate inhibition of the NF-κB pathway. In addition to the catalytic subunits of the IKK complex, NEMO is itself phosphorylated on multiple residues by several proteins kinases (57). These phosphorylation events serve to regulate NEMO function and inflammatory signaling. It will be of interest to determine whether NEMO is also a target for ST-associated protein phosphatases in MCPyV-expressing cells.

In contrast to MCPyV, SV40 promotes NF-κB activation via PP2A, although expression of proinflammatory cytokines and major histocompatibility complex class I molecules is also downregulated (30). The interaction of SV40 ST with PP2A results in increased protein kinase C signaling and upregulated Akt activity. This leads to activation of NF-κB and confers cellular resistance to apoptosis (58). Recent work comparing MCPyV-negative and MCPyV-positive tumors has shown that both tumor sets are indistinguishable in terms of histological and clinical features. However, no MCPyV-positive tumors present phosphatidylinositol 3-kinase (PI3K)/pAKT activation, while a subset of MCPyV-negative tumors contains PI3K-activating mutations (59). Moreover, MCPyV ST-induced cellular transformation is independent of the conserved polyomavirus ST interaction with PP2A. It is possible that MCPyV-mediated tumorigenesis occurs via an alternative cellular signaling pathway or as a result of other genetic abnormalities. Therefore, we employed a quantitative SILAC-based immunoprecipitation technique coupled to mass spectrometry to facilitate the detection of proteins in substoichiometric amounts or binding with lower affinity in multiprotein complexes (47). Results show that MCPyV ST interacts with the PP2A Aα subunit as

previously reported (14); however, a stronger association was observed with PP4C and PP2A Aβ subunits. SV40 ST binds the PP2A Aα subunit, while murine polyomavirus ST is known to interact with both PP2A subunits (60). Current evidence suggests that PP2A Aβ isoforms act as major tumor suppressor. Although expressed at lower levels in human cells than Aα isoforms, they are more commonly mutated in a number of different cancers (61, 62). Interaction with this subunit may implicate alternative cellular signaling pathways associated with MCC. More surprising was the association between MCPyV ST and the catalytic subunit of PP4. Although polyomavirus ST antigens have been reported to make contact with the PP2A C subunit, due to A subunit interactions (63), binding to the catalytic subunit of other major cellular phosphatases has not been previously demonstrated. This raises the question whether MCPyV ST and PP4C directly interact or if PP4C is part of a complex containing MCPyV ST and PP2A Aβ. Of possible relevance is the finding that protein phosphatase 5 (PP5) interacts with the PP2A A and B subunits (64). PP5 differs from the other serine/threonine phosphatases, as its regulatory and catalytic regions are encoded within a single polypeptide chain (65). However, the PP5 catalytic region is related to the PP2A catalytic subunit and therefore can be incorporated into a heterotrimeric complex with the PP2A A and B subunits (64). As incorporation of the catalytic subunit of PP4 in this manner has not been reported, these results may implicate a novel function for PP2A complexes as well as polyomavirus ST proteins. Interestingly, a similar mechanism may be employed by G protein, beta-subunit like (GβL), a member of the WD repeat-containing family which is involved in various intracellular signaling events. Recent studies suggest that GβL interacts with PP2A and PP6 and functions as a negative regulator of NF-κB signaling by recruiting protein phosphatases to the IKK complex (66). Further work will distinguish the roles of each of the phosphatase subunits bound by ST; however, these data do raise the exciting possibility that distinct pools of ST protein complexes within the cell, each bound by a different phosphatase and performing a specific function, may exist. In this regard, the use of the R7A mutation, which ablates binding to PP2A Aα, has been essential to exclude this phosphatase from the immunomodulatory effects described in this study. More refined mutations that are able to distinguish between PP2A Aβ and PP4C will allow further dissection of the function of these phosphatases in the MCPyV life cycle.

In summary, these findings highlight a novel and important role of MCPyV ST to subvert the innate immune response, allowing establishment of early or persistent infection within the host cell.

ACKNOWLEDGMENTS

We are indebted to Stefan Strack, University of Iowa, and Marilyn Goudrealt, University of Toronto, for kindly providing reagents. We also thank Julia Newton-Bishop for help with sample collection, Jamel Mankouri (Royal Society Research Fellow), and Gareth Howell, Leeds Bioimaging and Flow Cytometry Facility, for useful advice.

This work was supported in part by the British Skin Foundation, a BBSRC DTG studentship and research development fellowship, Cancer Research United Kingdom, Yorkshire Cancer Research, and a College of Pharmacy, University of Basrah, Ministry of Higher Education and Scientific Research Iraq, scholarship.

REFERENCES

1. **Becker JC, Schrama D, Houben R.** 2009. Merkel cell carcinoma. Cell. Mol. Life Sci. **66:**1–8.
2. **Agelli M, Clegg LX.** 2003. Epidemiology of primary Merkel cell carcinoma in the United States. J. Am. Acad. Dermatol. **49:**832–841.
3. **Engels EA, Frisch M, Goedert JJ, Biggar RJ, Miller RW.** 2002. Merkel cell carcinoma and HIV infection. Lancet **359:**497–498.
4. **Penn I, First MR.** 1999. Merkel's cell carcinoma in organ recipients: report of 41 cases. Transplantation **68:**1717–1721.
5. **Feng H, Shuda M, Chang Y, Moore PS.** 2008. Clonal integration of a polyomavirus in human Merkel cell carcinoma. Science **319:**1096–1100.
6. **Shuda M, Feng H, Kwun HJ, Rosen ST, Gjoerup O, Moore PS, Chang Y.** 2008. T antigen mutations are a human tumor-specific signature for Merkel cell polyomavirus. Proc. Natl. Acad. Sci. U. S. A. **105:**16272–16277.
7. **zur Hausen H.** 2008. Novel human polyomaviruses—Re-emergence of a well known virus family as possible human carcinogens. Int. J. Cancer **123:**247–250.
8. **Houben R, Shuda M, Weinkam R, Schrama D, Feng H, Chang Y, Moore PS, Becker JC.** 2010. Merkel cell polyomavirus-infected Merkel cell carcinoma cells require expression of viral T antigens. J. Virol. **84:**7064–7072.
9. **Bikel I, Loeken MR.** 1992. Involvement of simian virus-40 (Sv40) small T-antigen in transactivation of Sv40 early and late promoters. J. Virol. **66:**1489–1494.
10. **Cicala C, Avantaggiati ML, Graessmann A, Rundell K, Levine AS, Carbone M.** 1994. Simian-virus-40 small-T antigen stimulates viral DNA replication in permissive monkey cells. J. Virol. **68:**3138–3144.
11. **Moens U, Van Ghelue M, Johannessen M.** 2007. Oncogenic potentials of the human polyomavirus regulatory proteins. Cell. Mol. Life Sci. **64:**1656–1678.
12. **Sablina AA, Hahn WC.** 2008. SV40 small T antigen and PP2A phosphatase in cell transformation. Cancer And Metastasis Rev. **27:**137–146.
13. **Arroyo JD, Hahn WC.** 2005. Involvement of PP2A in viral and cellular transformation. Oncogene **24:**7746–7755.
14. **Shuda M, Kwun HJ, Feng H, Chang Y, Moore PS.** 2011. Human Merkel cell polyomavirus small T antigen is an oncoprotein targeting the 4E-BP1 translation regulator. J. Clin. Invest. **121:**3623–3634.
15. **Kwun HJ, Shuda M, Feng H, Camacho CJ, Moore PS, Chang Y.** 2013. Merkel cell polyomavirus small T antigen controls viral replication and oncoprotein expression by targeting the cellular ubiquitin ligase SCF(Fbw7). Cell Host Microbe **14:**125–135.
16. **Richards KH, Macdonald A.** 2011. Putting the brakes on the anti-viral response: negative regulators of type I interferon (IFN) production. Microbes Infect. **13:**291–302.
17. **Gilmore TD, Herscovitch M.** 2006. Inhibitors of NF-kappa B signaling: 785 and counting. Oncogene **25:**6887–6899.
18. **Karin M, Ben-Neriah Y.** 2000. Phosphorylation meets ubiquitination: the control of NF-kappa B activity. Annu. Rev. Immunol. **18:**621–663.
19. **Wu CJ, Conze DB, Li T, Srinivasula SM, Ashwell JD.** 2006. Sensing of Lys 63-linked polyubiquitination by NEMO is a key event in NF-kappaB activation. Nat. Cell Biol. **8:**398–406.
20. **Scheidereit C.** 2006. IkappaB kinase complexes: gateways to NF-kappaB activation and transcription. Oncogene **25:**6685–6705.
21. **Hayden MS, Ghosh S.** 2004. Signaling to NF-kappa B. Genes Dev. **18:**2195–2224.
22. **Le Negrate G.** 2012. Viral interference with innate immunity by preventing NF-kappaB activity. Cell. Microbiol. **14:**168–181.
23. **Joo MS, Hahn YS, Kwon MJ, Sadikot RT, Blackwell TS, Christman JW.** 2005. Hepatitis C virus core protein suppresses NF-kappa B activation and cyclooxygenase-2 expression by direct interaction with I kappa B kinase beta. J. Virol. **79:**7648–7657.
24. **Spitkovsky D, Hehner SP, Hofmann TG, Moller A, Schmitz ML.** 2002. The human papillomavirus oncoprotein E7 attenuates NF-kappa B activation by targeting the I kappa B kinase complex. J. Biol. Chem. **277:**25576–25582.
25. **Randall CM, Jokela JA, Shisler JL.** 2012. The MC159 protein from the molluscum contagiosum poxvirus inhibits NF-kappaB activation by interacting with the IkappaB kinase complex. J. Immunol. **188:**2371–2379.
26. **Fliss PM, Jowers TP, Brinkmann MM, Holstermann B, Mack C, Dickinson P, Hohenberg H, Ghazal P, Brune W.** 2012. Viral mediated redirection of NEMO/IKKgamma to autophagosomes curtails the inflammatory cascade. PLoS Pathog. **8:**e1002517.

27. **Powell PP, Dixon LK, Parkhouse RME.** 1996. An I kappa B homolog encoded by African swine fever virus provides a novel mechanism for downregulation of proinflammatory cytokine responses in host macrophages. J. Virol. **70:**8527–8533.
28. **Tait SWG, Reid EB, Greaves DR, Wileman TE, Powell PP.** 2000. Mechanism of inactivation of NF-kappa B by a viral homologue of I kappa B alpha-signal-induced release of I kappa B alpha results in binding of the viral homologue to NF-kappa B. J. Biol. Chem. **275:**34656–34664.
29. **Camus-Bouclainville C, Fiette L, Bouchiha S, Pignolet A, Counor D, Filipe U, Gelfi J, Messud-Petit F.** 2004. A virulence factor of myxoma virus colocalizes with NF-kappa B in the nucleus and interferes with inflammation. J. Virol. **78:**2510–2516.
30. **Moreno CS, Ramachandran S, Ashby DG, Laycock N, Plattner CA, Chen W, Hahn WC, Pallas DC.** 2004. Signaling and transcriptional changes critical for transformation of human cells by simian virus 40 small tumor antigen or protein phosphatase 2A B56 gamma knockdown. Cancer Res. **64:**6978–6988.
31. **Jackson BR, Boyne JR, Noerenberg M, Taylor A, Hautbergue GM, Walsh MJ, Wheat R, Blackbourn DJ, Wilson SA, Whitehouse A.** 2011. An interaction between KSHV ORF57 and UIF provides mRNA-adaptor redundancy in herpesvirus intronless mRNA export. PLoS Pathog. **7:**e1002138.
32. **Mankouri J, Fragkoudis R, Richards KH, Wetherill LF, Harris M, Kohl A, Elliott RM, Macdonald A.** 2010. Optineurin negatively regulates the induction of IFN beta in response to RNA virus infection. PLoS Pathog. **6:**e1000778.
33. **Macdonald A, Crowder K, Street A, McCormick C, Saksela K, Harris M.** 2003. The hepatitis C virus non-structural NS5A protein inhibits activating protein-1 function by perturbing ras-ERK pathway signaling. J. Biol. Chem. **278:**17775–17784.
34. **Gould F, Harrison SM, Hewitt EW, Whitehouse A.** 2009. Kaposi's sarcoma-associated herpesvirus RTA promotes degradation of the Hey1 repressor protein through the ubiquitin proteasome pathway. J. Virol. **83:**6727–6738.
35. **Hall KT, Stevenson AJ, Goodwin DJ, Gibson PC, Markham AF, Whitehouse A.** 1999. The activation domain of herpesvirus saimiri R protein interacts with the TATA-binding protein. J. Virol. **73:**9756–7337.
36. **Boyne JR, Jackson BR, Taylor A, Macnab SA, Whitehouse A.** 2010. Kaposi's sarcoma-associated herpesvirus ORF57 protein interacts with PYM to enhance translation of viral intronless mRNAs. EMBO J. **29:**1851–1864.
37. **Goodwin DJ, Whitehouse A.** 2001. A gamma-2 herpesvirus nucleocytoplasmic shuttle protein interacts with importin alpha 1 and alpha 5. J. Biol. Chem. **276:**19905–19912.
38. **Griffiths R, Whitehouse A.** 2007. Herpesvirus saimiri episomal persistence is maintained via interaction between open reading frame 73 and the cellular chromosome-associated protein MeCP2. J. Virol. **81:**4021–4032.
39. **Hall KT, Giles MS, Calderwood MA, Goodwin DJ, Matthews DA, Whitehouse A.** 2002. The herpesvirus saimiri open reading frame 73 gene product interacts with the cellular protein p32. J. Virol. **76:**11612–11622.
40. **Emmott E, Rodgers MA, Macdonald A, McCrory S, Ajuh P, Hiscox JA.** 2010. Quantitative proteomics using stable isotope labeling with amino acids in cell culture reveals changes in the cytoplasmic, nuclear, and nucleolar proteomes in Vero cells infected with the coronavirus infectious bronchitis virus. Mol. Cell. Proteomics **9:**1920–1936.
41. **Jourdan SS, Osorio F, Hiscox JA.** 2012. An interactome map of the nucleocapsid protein from a highly pathogenic North American porcine reproductive and respiratory syndrome virus strain generated using SILAC-based quantitative proteomics. Proteomics **12:**1015–1023.
42. **Taylor A, Jackson BR, Noerenberg M, Hughes DJ, Boyne JR, Verow M, Harris M, Whitehouse A.** 2011. Mutation of a C-terminal motif affects Kaposi's sarcoma-associated herpesvirus ORF57 RNA binding, nuclear trafficking, and multimerization. J. Virol. **85:**7881–7891.
43. **Huang TT, Wuerzberger-Davis SM, Wu Z-H, Miyamoto S.** 2003. Sequential modification of NEMO/IKKgamma by SUMO-1 and ubiquitin mediates NF-kappaB activation by genotoxic stress. Cell **115:**565.
44. **Jager S, Bucci C, Tanida I, Ueno T, Kominami E, Saftig P, Eskelinen EL.** 2004. Role for Rab7 in maturation of late autophagic vacuoles. J. Cell Sci. **117:**4837–4848.
45. Deretic V. 2008. Autophagosome and phagosome. Methods Mol. Biol. **445:**1–10.
46. **Cheng J, DeCaprio JA, Fluck MM, Schaffhausen BS.** 2009. Cellular transformation by simian virus 40 and murine polyoma virus T Antigens. Semin. Cancer Biol. **19:**218–228.
47. **Trinkle-Mulcahy L, Boulon S, Lam YW, Urcia R, Boisvert FM, Vandermoere F, Morrice NA, Swift S, Rothbauer U, Leonhardt H, Lamond A.** 2008. Identifying specific protein interaction partners using quantitative mass spectrometry and bead proteomes. J. Cell Biol. **183:**223–239.
48. **Munday DC, Surtees R, Emmott E, Dove BK, Digard P, Barr JN, Whitehouse A, Matthews D, Hiscox JA.** 2012. Using SILAC and quantitative proteomics to investigate the interactions between viral and host proteomes. Proteomics **12:**666–672.
49. **Arora R, Shuda M, Guastafierro A, Feng H, Toptan T, Tolstov Y, Normolle D, Vollmer LL, Vogt A, Domling A, Brodsky JL, Chang Y, Moore PS.** 2012. Survivin is a therapeutic target in merkel cell carcinoma. Sci. Transl. Med. **4:**133–156.
50. **Hein J, Boichuk S, Wu J, Cheng Y, Freire R, Jat PS, Roberts TM, Gjoerup OV.** 2009. Simian virus 40 large T antigen disrupts genome integrity and activates a DNA damage response via Bub1 binding. J. Virol. **83:**117–127.
51. **Field N, Low W, Daniels M, Howell S, Daviet L, Boshoff C, Collins M.** 2003. KSHV vFLIP binds to IKK-gamma to activate IKK. J. Cell Sci. **116:**3721–3728.
52. **Shembade N, Harhaj NS, Yamamoto M, Akira S, Harhaj EW.** 2007. The human T-cell leukemia virus type 1 tax oncoprotein requires the ubiquitin-conjugating enzyme Ubc13 for NF-kappa B activation. J. Virol. **81:**13735–13742.
53. **Li HY, Liu H, Wang CH, Zhang JY, Man JH, Gao YF, Zhang PJ, Li WH, Zhao J, Pan X, Zhou T, Gong WL, Li AL, Zhang XM.** 2008. Deactivation of the kinase IKK by CUEDC2 through recruitment of the phosphatase PP1. Nat. Immunol. **9:**533–541.
54. **Li S, Wang L, Berman MA, Zhang Y, Dorf ME.** 2006. RNAi screen in mouse astrocytes identifies phosphatases that regulate NF-kappaB signaling. Mol. Cell **24:**497–509.
55. **Brechmann M, Mock T, Nickles D, Kiessling M, Weit N, Breuer R, Muller W, Wabnitz G, Frey F, Nicolay JP, Booken N, Samstag Y, Klemke CD, Herling M, Boutros M, Krammer PH, Arnold R.** 2012. A PP4 holoenzyme balances physiological and oncogenic nuclear factor-kappa B signaling in T lymphocytes. Immunity **37:**697–708.
56. **Barisic S, Strozyk E, Peters N, Walczak H, Kulms D.** 2008. Identification of PP2A as a crucial regulator of the NF-kappaB feedback loop: its inhibition by UVB turns NF-kappaB into a pro-apoptotic factor. Cell Death Differ. **15:**1681–1690.
57. **Clark K, Nanda S, Cohen P.** 2013. Molecular control of the NEMO family of ubiquitin-binding proteins. Nat. Rev. Cancer **13:**673–685.
58. **Sontag E, Sontag JM, Garcia A.** 1997. Protein phosphatase 2A is a critical regulator of protein kinase C zeta signaling targeted by SV40 small t to promote cell growth and NF-kappa B activation. EMBO J. **16:**5662–5671.
59. **Nardi VSY, Santamaria-Barria JA, Cosper AK, Lam Q, Faber AC, Boland GM, Yeap BY, Bergethon K, Scialabba VL, Tsao H, Settleman J, Ryan DP, Borger DR, Bhan AK, Hoang MP, Iafrate AJ, Cusack JC, Engelman JA, Dias-Santagata D.** 2012. Activation of PI3K signaling in Merkel cell carcinoma. Clin. Cancer Res. **18:**1227–1236.
60. **Andrabi S, Hwang JH, Choe JK, Roberts TM, Schaffhausen BS.** 2011. Comparisons between murine polyomavirus and simian virus 40 show significant differences in small T antigen function. J. Virol. **85:**10649–10658.
61. **Janssens V, Goris J.** 2001. Protein phosphatase 2A: a highly regulated family of serine/threonine phosphatases implicated in cell growth and signalling. Biochem. J. **353:**417–439.
62. **Wang SS, Esplin ED, Li JL, Huang LY, Gazdar A, Minna J, Evans GA.** 1998. Alterations of the PPP2R1B gene in human lung and colon cancer. Science **282:**284–287.
63. **Yang SI, Lickteig RL, Estes R, Rundell K, Walter G, Mumby MC.** 1991. Control of protein phosphatase-2a by simian virus-40 small-T antigen. Mol. Cell. Biol. **11:**1988–1995.
64. **Lubert EJ, Hong YL, Sarge KD.** 2001. Interaction between protein phosphatase 5 and the A subunit of protein phosphatase 2A—evidence for a heterotrimeric form of protein phosphatase 5. J. Biol. Chem. **276:**38582–38587.
65. **Skinner J, Sinclair C, Romeo C, Armstrong D, Charbonneau H, Rossie S.** 1997. Purification of a fatty acid-stimulated protein-serine/threonine phosphatase from bovine brain and its identification as a homolog of protein phosphatase 5. J. Biol. Chem. **272:**22464–22471.
66. **You DJ, Kim YL, Park CR, Kim DK, Yeom J, Lee C, Ahn C, Seong JY, Hwang JI.** 2010. Regulation of IkappaB kinase by GbetaL through recruitment of the protein phosphatases. Mol. Cells **30:**527–532.